

Single-Crystal Silicon Nanotubes, Hollow Nanocones, and Branched Nanotube Networks

Corey P. Fucetola, Justin T. Wang, Olurotimi A. Bolonduro, Charles M. Lieber,* and Brian P. Timko*



Cite This: *ACS Nano* 2024, 18, 3775–3782



Read Online

ACCESS |

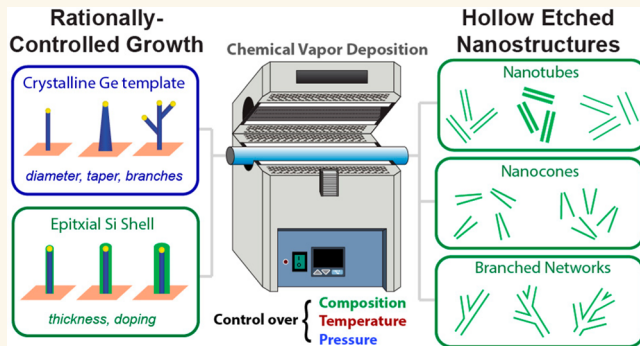
Metrics & More

Article Recommendations

Supporting Information

ABSTRACT: We report a general approach for the synthesis of single-crystal silicon nanotubes, involving epitaxial deposition of silicon shells on germanium nanowire templates followed by removal of the germanium template by selective wet etching. By exploiting advances in the synthesis of germanium nanowires, we were able to rationally tune the nanotube internal diameters (5–80 nm), wall thicknesses (3–12 nm), and taper angles (0–9°) and additionally demonstrated branched silicon nanotube networks. Field effect transistors fabricated from p-type nanotubes exhibited a strong gate effect, and fluid transport experiments demonstrated that small molecules could be electrophoretically driven through the nanotubes. These results demonstrate the suitability of silicon nanotubes for the design of nanoelectrofluidic devices.

KEYWORDS: Nanowires, Nanotubes, Silicon, Germanium, Core–shell, nanofluidics



Synthetic nanoscale tubes, channels, and pores have broad applications in energy storage^{1,2} and bioscience, with examples including intracellular electrophysiology,^{3–7} nucleic acid sequencing,⁸ pathogen detection (including SARS-CoV-2⁹), and drug delivery.¹⁰ Nonlayered inorganic tubes composed of metal,^{11,12} oxides,^{13–16} undoped Si,^{17–19} Si carbide,²⁰ and group III–V semiconductors^{21–24} have been reported. Hollow single-crystal semiconductor nanostructures could offer distinct applications including integrated sensing^{7,25} and fluid transport devices with electrolytic conductance tunable through local electrostatic gating^{26–28} or chemical surface modification.²⁹ They could also form stable bioelectronic interfaces with the cellular cytosol, allowing for patch clamp-like bioelectronic readouts.³⁰ The bottom-up synthesis of such nanostructures could offer rational control over design parameters such as channel width (nanotube internal diameter), diffuser/nozzle opening angle (hollow nanocone taper angle), and junction geometry (nanotube branch diameter and angle).³¹ At the same time, fine control over wall diameter, single-crystallinity, and doping would impart advantages similar to those demonstrated with electrically based nanowire sensors.⁷ However, a synthetic route toward hybrid structures with control over both the geometric and electrical properties has not been demonstrated to date.

Inorganic nanotubes have been prepared previously by a variety of techniques, including sol–gel chemistry,^{13,32} electroless deposition,¹¹ catalyst-assisted chemical vapor deposition (CVD)¹⁸ inside porous alumina membranes, molecular beam epitaxy atop alumina membranes,¹⁷ electrochemical anodization of porous aluminum films,¹⁶ diffusion-limited vapor–liquid–solid (VLS) growth,²⁴ and in situ chemical conversion of existing nanotubes.²¹ Each of these approaches is either intolerant of dopants or limits the structural diversity of tubes to the shapes of available membranes or preexisting structures. A more versatile method is to grow a nanowire template, the size and shape of which are readily controlled. Tubes can then be formed by uncatalyzed CVD,^{19,22} atomic layer deposition,¹⁴ or metalorganic vapor phase epitaxy²³ of shells on the template followed by wet etching of the template cores, or by vapor–solid reactions with the template followed by burn off of

Received: November 27, 2023

Revised: January 8, 2024

Accepted: January 10, 2024

Published: January 16, 2024



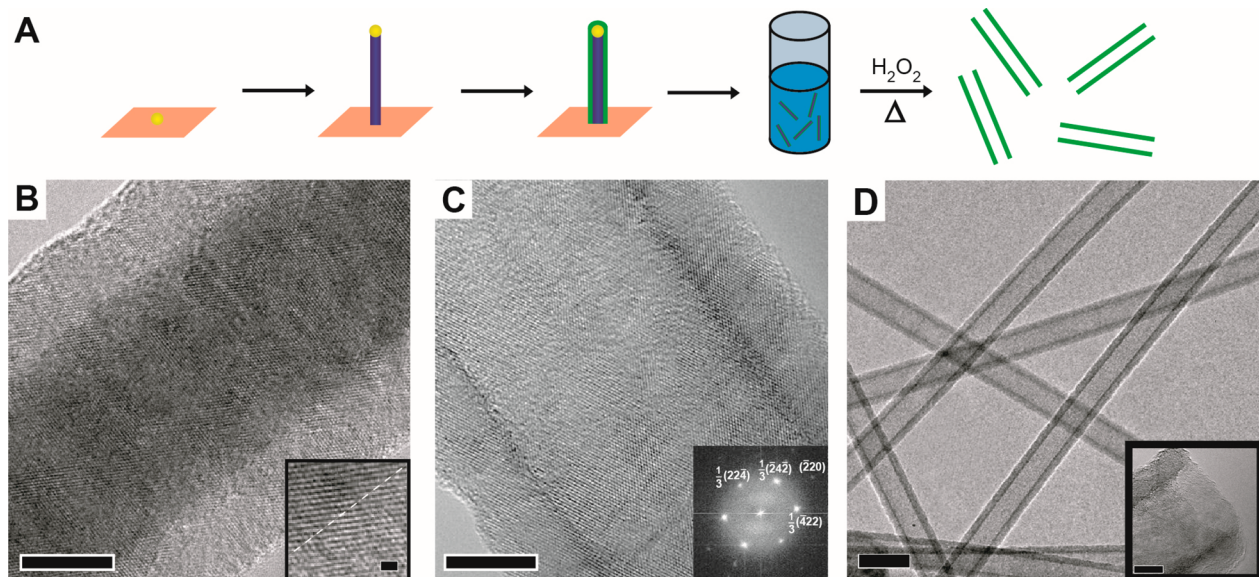


Figure 1. Synthesis and transmission electron microscopy. (A) Nanotubes are produced by growing Ge nanowires (blue) and then coating with Si shells (green). The nanostructures are removed from the substrate by sonication, and then, the Ge is etched in a heated H_2O_2 solution. (B) High resolution TEM image showing that an intrinsic Si shell forms uniformly and epitaxially on a Ge core. Scale bar is 10 nm. (inset) Enlargement of interface region showing sharp epitaxy. Scale bar is 1 nm. (C) High resolution TEM of a nanotube demonstrates that the etch process does not disturb the crystallinity of the Si wall. Scale bar is 10 nm. (inset) Two-dimensional Fourier transform of the image. (D) After etching, Si tubes of uniform geometry remain. Scale bar is 50 nm. (inset) The open end of a typical nanotube exhibits a hollow core and stable wall. Scale bar is 5 nm.

unreacted core material.²⁰ We used the first approach because it allows greater versatility in the shell material.

RESULTS AND DISCUSSION

Silicon Nanotubes Are Single-Crystalline and Exhibit Tunable Electrical Transport. We synthesized single-crystalline Si nanotubes by uncatalyzed CVD on a Ge nanowire template. We chose this method since the size, shape, and geometry of the Ge template can be rationally controlled, and since a nanoscale layer of Si can be deposited epitaxially onto Ge.^{33,34} The Ge template was selectively etched³⁵ by heated H_2O_2 (65°C), leaving the Si shell intact (Figure 1A). Transmission electron microscopy (TEM) of the unetched heterostructures showed that growth occurred along the $\langle 100 \rangle$ (5%), $\langle 110 \rangle$ (33%), $\langle 111 \rangle$ (5%), and $\langle 112 \rangle$ (57%) directions, as reported previously for Si.³⁰ Images of the core–shell wires confirm that the growth is epitaxial with a clean interface between Ge and Si (Figure 1B). A 2D-Fourier transform was performed locally on Ge and Si image regions, showing that both are along the $\langle 112 \rangle$ direction (Figure S1). The ratios of d spacings $d_{\text{Ge}}/d_{\text{Si}}$ were 1.029 ± 0.022 , 1.035 ± 0.005 , and 1.034 ± 0.002 for the $1/3\{422\}$, $\{220\}$, and $2/3\{422\}$ reflections, respectively (Figure S1). These are similar to but systematically lower than the expected ratio of 1.040 for bulk materials,³⁷ suggesting that strain is present in the structure. A high-resolution image of an etched nanotube (Figure 1C) confirms that the crystallinity of the shell was unaffected by the etch. A 2D Fourier transform of the image (Figure 1C, inset) indicates that the growth direction of the template was also along the $\langle 112 \rangle$ axis. These nanotubes were highly uniform (Figure 1D) with open ends (Figure 1D, inset), and few catalyst particles were found.

Whereas past studies have dealt with the sensing of molecules and biological species bound to semiconducting nanowire devices,²⁵ these Si nanotubes might prove more

sensitive because each analyte molecule passing through a tube would lie within one Debye length of the sensing device.²⁶ Unlike intrinsic core/shell Ge/Si nanowires, which can conduct ballistically,³³ undoped Si shells alone are insulating. We hypothesized that boron-doped single-crystal Si nanotubes could function as p-channel field effect transistors (FETs), as observed previously with Si-nanowire FETs.^{7,25} Figure 2 shows the drain-source current (I_{ds}) versus bias voltage (V_{ds}) for a typical nanotube device (grown with a Si/B feed ratio of 1500:1), with Ni source and drain contacts defined by electron beam microscopy (Figure 2, lower inset). To measure the gate response of these tubes, we measured I_{ds} versus back gate potential (V_g) at a constant drain-source bias ($V_{\text{ds}} = -1$ V). The representative device shown exhibited characteristic FET behavior,^{38,39} in which the current turned off around $V_g = 1$ V (Figure 2, upper inset). I_{ds} vs V_g was analyzed in the linear region well-above threshold between -6.5 and -9 V and yielded a transconductance $-I_{\text{ds}}/V_g = 119$ nS. Because the measurements were performed on doped Si nanotubes using a relatively thick and low dielectric constant (50 nm SiO_2) back-gate geometry, the mobility was analyzed using a classical cylinder and infinite plate model (see Methods). This analysis yielded a hole mobility of $\mu = 20.6 \text{ cm}^2/\text{V}\cdot\text{s}$ that is within the range of values reported for SiNW FETs.³⁸

Size and Shape Can Be Rationally Controlled. An advantage of our synthetic approach is that it enables independent control over the internal diameter, wall thickness, and doping. To measure the precision of the growth technique, we grew and analyzed samples using a variety of catalyst sizes and shell deposition times. Tubes grown using 5, 20, and 80 nm catalyst particles (Figure 3A–C) were found to have uniform internal diameters of 7.2 ± 1.7 , 19.2 ± 2.5 , and 75.6 ± 4.3 nm, respectively. Shells deposited on 10 nm cores for 5, 20, and 50 min (Figure 3D–F) were found to have thicknesses of 3.4 ± 0.5 , 5.1 ± 0.3 , and 12.3 ± 0.9 nm, confirming that shell

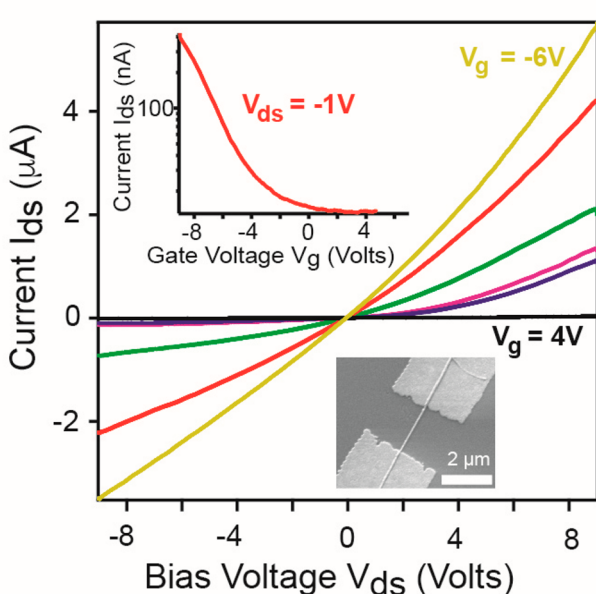


Figure 2. Electrical transport of p-type nanotubes. Single nanotube transport measurements show typical p-channel FET behavior. Curves were recorded at equally spaced gate voltages ranging from $V_g = 4\text{ V}$ (black) to $V_g = -6\text{ V}$ (yellow). (upper inset) Current (I_{ds}) vs gate voltage (V_g) for the same device recorded at a drain bias of $V_{ds} = -1\text{ V}$; note that the current can be completely turned off. (lower inset) Scanning electron micrograph (SEM) of actual device. The channel length is $2\text{ }\mu\text{m}$.

thickness is a monotonic function of deposition time. The growth rate slows with increased shell thickness, as expected for depletion of available reactant gas at a growing interface.⁴⁰ This type of precise control over tube geometry might enable size and conformation selection of passing molecules, a desirable attribute for biotechnological applications like nanopore DNA sequencing.⁴¹

Notably, our approach can also be readily extended to produce a variety of other hollow nanostructures. Hollow cones were templated from tapered Ge nanowires formed through simultaneous catalyzed axial elongation and uncatalyzed radial growth (Figure 4A). Such radial growth is promoted by vapor deposition at higher temperatures and GeH_4 partial pressures than those used for nontapered cores (see Methods). The cone angle increases with the core growth temperature, a result of faster overcoating relative to axial elongation. Cone taper angles at growth temperatures of 380 and $400\text{ }^\circ\text{C}$ (Figure 4B,C) were, respectively, measured to be $3.2 \pm 0.7^\circ$ and $8.6 \pm 2.2^\circ$, indicating that the angle could be controlled by deposition temperature. At the higher temperature, the growth substrate was also overcoated with Ge, leading to cones connected by free-standing Si films (Figure 4C, inset) of up to several square millimeters in area. The size scale of these devices is relevant for filtering applications, including ion-rectified membranes which require asymmetrically shaped pores.⁴² Structures with programmable tapers could also lead to advances in bioelectronics studies, analogously to mushroom-shaped electrodes which were engulfed by cells for intracellular recordings.⁴³

Si nanotubes could form functional elements in nanofluidic circuits.⁴⁴ To explore the possibility of forming Si nanotube junctions, we deposited Si shells on branched Ge templates,

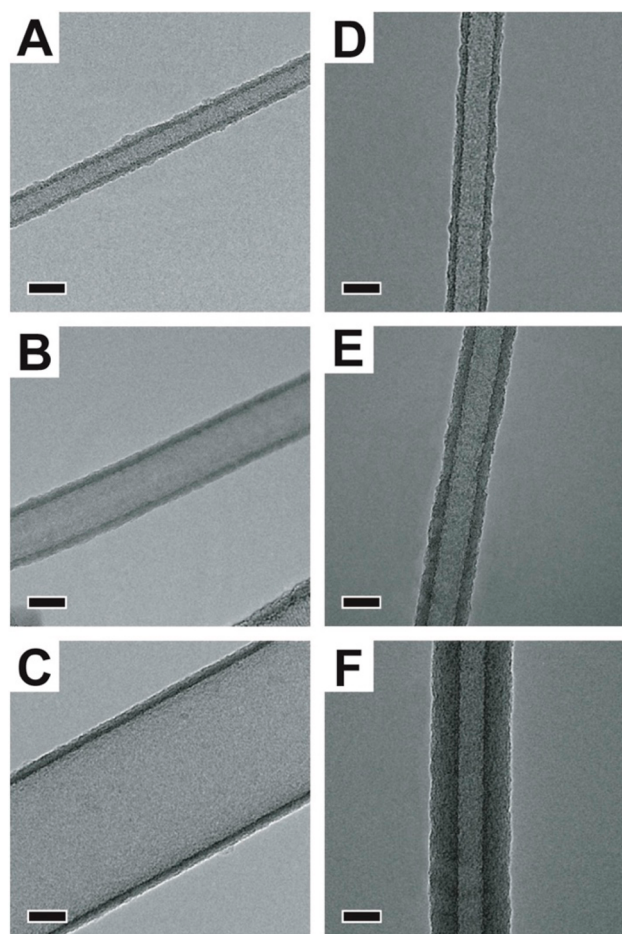


Figure 3. Nanotubes with rationally tuned size. Si nanotubes having internal diameters of (A) 5, (B) 20, and (C) 80 nm were synthesized using Au catalyst particles of the desired diameter. Control of wall thickness was also demonstrated by CVD deposition of the shell for (D) 5, (E) 20, and (F) 50 min. All scale bars are 20 nm.

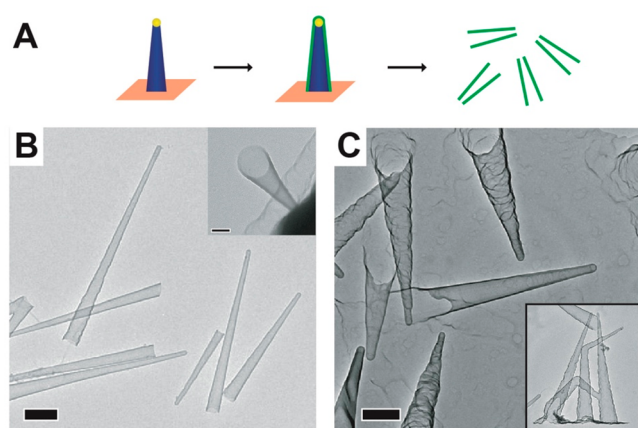


Figure 4. Hollow nanocones. (A) Scheme representing hollow Si nanocone growth from tapered Ge template. (B,C) Nanocones templated from highly tapered Ge cores grown at (B) 380 and (C) $400\text{ }^\circ\text{C}$. Scale bars are 200 nm. (B, inset) The base of a typical cone, viewed at an oblique angle, is circular and open (scale bar, 200 nm). (C, inset) Nanocones grown at $400\text{ }^\circ\text{C}$ are connected by a solid Si film.

similar to those reported previously with Si.^{45,46} Briefly, untapered Ge wires were grown by the same process as described earlier. The sample was removed from the furnace, and Au catalyst particles were randomly deposited from aqueous suspension on the wire surface. The chip was then returned to the furnace for branch growth followed by conformal deposition of the Si shell as described previously (Figure 5A). We found that the apertures between backbone

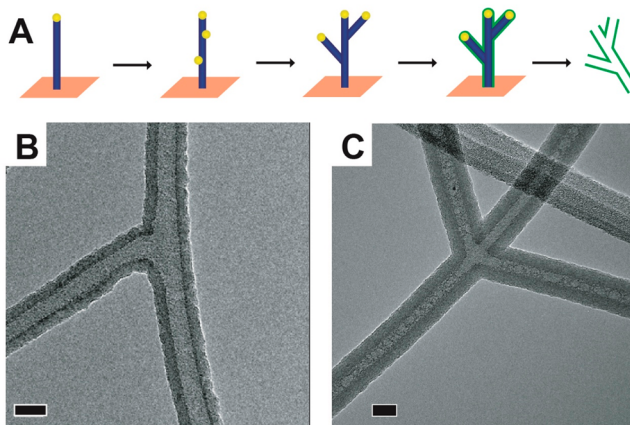


Figure 5. Branched nanotubes. (A) Scheme representing branched Si nanotube growth from a branched Ge nanowire template. (B, C) The heterostructures were etched to yield branched Si nanotube networks with open junctions. Examples of singly and doubly branched nanotubes are shown. Scale bars are 20 nm.

and branch nanotubes were fully open (Figure 5B). Using a higher catalyst density resulted in multiple branches within the proximity of each other (Figure 5C). In fully open branched structures, we found a distribution of angles (Figure S2) between the branches and the backbones consistent with previously reported branch angles of 35.3°, 54.7°, 70.5°, and 90° for Si wires epitaxially grown from Si nanowire backbones⁴⁵ and (100), (110), and (111) Si wafers.⁴⁷ In addition to passive microfluidic integration, these branches could be useful for actively controlling fluid delivery in well-defined directions by selectively pinching off ionic flows with local electrical gates.^{26,27}

Silicon Nanotubes Enable Nanofluidic Transport. An important property of nanoscale channels is that the charge bilayer can span the channel rather than merely defining the boundary layer, although the exact dynamics of such confined ion flows are still under investigation.^{27,44} In a proof-of-concept experiment, a Si nanotube was used to connect two fluid reservoirs on a glass substrate (see **Methods**). The reservoirs were separated by a 10-μm-wide, 25-μm-tall polymer barrier, while a pair of lithographically defined Au electrodes imposed a DC field (Figure 6A,B). The reservoirs were filled with water with one side containing 90 μM Oregon Green 488 dye (2',7'-difluorofluorescein). Confocal microscopy was used to observe the fluorescence and hence the diffusion and migration of the dye. Before applying a field, the tube appeared dark (Figure 6C). Initially, the dye did not diffuse into the tube because of repulsive forces between the negatively charged molecule and the oxidized Si surface. Applying a field of 10 kV/cm across the tube drove the dye through the structure. Fluorescence was observed clearly through the wall of the tube (Figure 6D, **Supporting Information Movie**) as well as at the

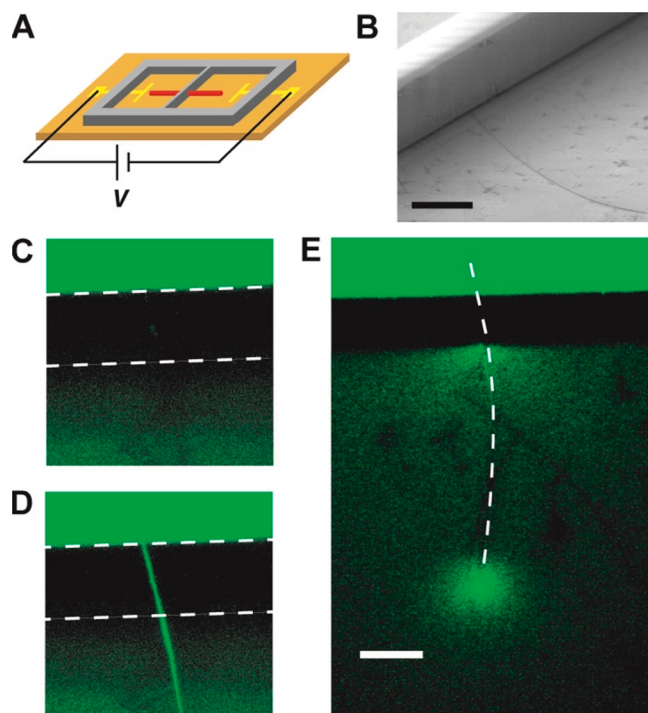


Figure 6. Nanofluidic transport. (A) Schematic of a single nanotube device with fluid reservoirs on either end. (B) SEM of a representative nanotube device taken at a 45° tilt. Scale bar: 20 μm. (C) Epifluorescence microscopy was used to study the transport of dye between two reservoirs via tubes. Initially, the tube did not contain dye. (D) When an electric field was applied, the dye solution filled the tube and was transported to the other (water-filled) reservoir. The dotted line shows the position of the SU8 barrier. (E) Image of the same tube, showing diffusion of dye away from the open end. The dotted line shows the position of the tube. Scale bar is 10 μm.

open end (Figure 6E) where the dye diffused into the water-filled reservoir.

CONCLUSIONS

We demonstrated the rational synthesis of single-crystal Si nanotubes, nanocones, and branched nanofluidic networks. Owing to the flexibility of our Ge nanowire-templated approach, we achieved these hollow nanostructures with rationally controlled doping and geometry, including diameter and wall thickness (nanotubes), taper angle (nanocones), and branch density (networks). Our electrical and fluid transport experiments demonstrate that integrated, Si-based nanofluidic devices could be capable of simultaneously transporting, processing, and sensing fluids on the subfemtoliter scale. These functionalities could be useful in biological applications such as nanomedicine, sequencing, and charge transport. In particular, Si nanotubes might act as synthetic ion channels that link extracellular electronics to the cytosol. Significantly, 1D nanostructures with dimensions similar to our tubes can stably⁴⁸ (and in some cases, spontaneously^{49,50}) penetrate the cell membrane, nanotubes can be functionalized or tapered⁴² to achieve ion selectivity, and nanotubes with chemical or electrical detection capabilities^{7,25} might be integrated with other nanoscale elements⁵¹ to regulate cellular function.

Nanofluidics is an emerging field, with nascent studies revealing surprising physical behaviors such as dielectric anomalies, ionic Coulomb blockade, and Coulomb drag

effects. If fully harnessed, nanofluidic physics could be transformative for fields such as water remediation and energy.⁴⁴ Our tunable nanotube networks could provide a platform for studying the physics of nanoconfined fluids, while hollow cone-shaped structures could provide “interconnects” between nano- and microscale systems.

Realizing these nanofluidic systems will require refined bottom-up assembly strategies. Examples of directed assembly approaches achieved for nanowires include alignment within microfluidic flows, electric fields, and blown films,⁵² assembly into lithographically defined trenches,^{53,54} and nanocombing techniques where anchored nanowires were drawn out onto a distinct target substrate.⁵⁵ The most recent approaches^{53–55} have enabled deterministic assembly and device integration at the single-nanowire level, enabling large organized arrays of functional transistors⁵³ and electromechanical resonators.⁵⁴ These assembly methods have also been expanded to achieve 3D, hierarchically structured nanowire assemblies⁵⁶ as well as a nanocomputer finite-state machine.⁵⁷ Further control over hollow Si architectures might be achieved with synthetic DNA templates, which can be encoded with spatial positioning information to achieve complex, self-assembled structures such as origami⁵⁸ or bricks.⁵⁹ The programmable self-organization of these DNA architectures has been leveraged to assemble solid-state nanomaterials in 3D configurations with nanometer-scale resolution.⁶⁰

Future iterations of nanotubes could be synthetically encoded with additional functionalities such as p/n junctions for electrical current rectification or photovoltaic current production,^{51,61} ultrathin dielectric layers to modulate transconductance and enhance longevity in aqueous media,⁶² and ultrasmall channel length FETs for low detection thresholds.⁴⁸ Nanotube-based devices might also be incorporated onto the ever-expanding repertoire of flexible^{63–65} and injectable scaffolds,^{7,66} enabling (bio)probes far smaller than current examples, where the lower size is limited by relatively large microelectrode devices.⁶⁷ The versatility and flexibility of our approach will allow for hollow nanomaterials with a wide variety of scientific and engineering applications.

METHODS

Silicon Nanotube Synthesis. Single-crystalline Ge nanowire templates were grown by the vapor–liquid–solid (VLS) process⁶⁸ from gold nanocluster catalysts in an atmosphere of 2.3% GeH₄ and a carrier gas of ultrapure H₂ at 300 Torr and 315 °C for a 1 min nucleation step, followed by 450 Torr and 280 °C for ca. 30 min of elongation. These conditions resulted in minimal overcoating of the wire from the uncatalyzed GeH₄ decomposition at the nanowire surface. Intrinsic Si shells were grown using SiH₄ reactant at 5 Torr and 450 °C, yielding a radial growth rate of ca. 0.5 nm/min, by uncatalyzed decomposition of the vapor on the Ge nanowire surface without promoting VLS growth of Ge/Si axial heterostructures.⁶⁹ Alternatively, p-type Si shells (1500:1) were grown using SiH₄ reactant (28%) and B₂H₆ (0.072%) dopant in ultrapure H₂ at 450 °C for 1 min while ramping pressure from 0 to ca. 20 Torr. A final annealing step was performed at 600 °C (intrinsic) or 800 °C (p-type) under vacuum for 2 h to fully crystallize the shell. Samples grown without annealing typically exhibited amorphous or polycrystalline shells. The resulting heterostructures were removed from the growth substrate by gentle sonication in 30% H₂O₂/H₂O solution. The solution was heated to 65 °C for ca. 1 h and then purified by at least two cycles of centrifugation at 14 krpm (10 min) and resuspension in ethanol.

Electrical Transport Measurements. Nanotube-based transistor devices were fabricated in a back-gate geometry.⁷⁰ Devices were

fabricated on a degenerately doped Si wafer, which served as the gate electrode, with a 50 nm thermal oxide layer as the gate dielectric. Purified nanotubes were dispersed on the Si/SiO_x substrate and located relative to a marker pattern, as determined by scanning electron microscopy. Ni electrical contacts (65 nm) were defined by electron beam lithography and deposited by thermal evaporation of the metal, then annealed at 350 °C for 60 s.

Mobility Calculations. We calculated the hole mobility from the transconductance

$$\mu = \frac{dI_{ds}}{dV_g} \left(\frac{L^2}{CV_{ds}} \right)$$

where L is the length of the nanotube, V_{ds} is the source/drain bias, and C is the capacitance of the thermal oxide layer. Because the measurements were performed on doped Si nanotubes using a relatively thick and low dielectric constant (50 nm SiO₂) back-gate geometry, and because the transconductance was measured at more than 1 V beyond the threshold voltage, the mobility was analyzed using a classical cylinder and infinite plate model

$$C \approx \frac{2\pi\epsilon\epsilon_0 L}{\cosh^{-1}(h/r)}$$

where ϵ and h are the relative permittivity and thickness of the oxide layer, respectively, and r is the outer radius of the nanotube.^{71,72} Setting $dI_{ds}/dV_g = -119$ nS, $L = 2 \mu\text{m}$, $V_{ds} = -1$ V, $\epsilon = 3.9$, $h = 50$ nm, and $r = 15$ nm, we found $C = 2.32 \times 10^{-16}$ F and $\mu = 20.6 \text{ cm}^2/\text{V}\cdot\text{s}$.

Silicon Nanocone Synthesis. Tapered Ge wires for conical shells were grown using Au nanocluster catalysts, with 10% GeH₄ reactant in H₂ carrier at 380–400 °C and 80 Torr. Growth occurred at a radial rate of about 10 nm/min and an axial rate of about 1 μm/min.

Structural Characterization. A JEOL 2010 field-emission TEM instrument was used for structure analyses. Nanostructures were released from the growth substrate by gentle sonication into ethanol and dispersed onto lacey carbon grids (Ted Pella). The high-resolution images shown in Figures 1B,C and S1 were measured along the [111] zone axis.

Nanofluidic Transport Measurements. Each reservoir measured 1 cm × 1 cm, and the wall separating the two chambers was 10 μm wide. The electrodes were 5 mm apart (with a separating barrier in the middle). Modeling the system as a series resistances, one can assume that nearly the entire potential drop occurred across the fluid-filled nanotube.

The substrates used were glass coverslips (Corning) upon which Au electrodes had previously been fabricated. First, Ge/Si heterostructure wires were deposited. The barriers were composed of SU8-25 (Kayaku Advanced Materials, Newton, MA), which was spin-coated (3000 rpm, 30 s) and exposed by photolithography. After development, the entire chip was hardbaked (180 °C for 30 min) to increase cross-linking of the polymer. Finally, the chips were submerged in 30% H₂O₂/H₂O for ca. 12 h at room temperature. Environmental Scanning Electron Microscopy (ESEM) with Energy-Dispersive X-ray Spectroscopy (EDS) detection was used to confirm that the Ge had been completely etched. The etched chip was mounted on an inverted lens confocal microscope with an epifluorescence capability. Oregon Green dye was excited using the 488 nm line of an argon ion laser, and fluorescence was observed through a 500–550 nm band-pass filter.

ASSOCIATED CONTENT

Supporting Information

The Supporting Information is available free of charge at <https://pubs.acs.org/doi/10.1021/acsnano.3c11841>.

Nanofluidic transport through Si nanotube (MP4)

Figures: Ge/Si interface, branch angle distributions (PDF)

AUTHOR INFORMATION

Corresponding Authors

Charles M. Lieber – Lieber Research Group, Lexington, Massachusetts 02420, United States;  orcid.org/0000-0002-6660-2456; Email: liebercharlesm@gmail.com

Brian P. Timko – Department of Biomedical Engineering, Tufts University, Medford, Massachusetts 02155, United States;  orcid.org/0000-0002-7958-8980; Email: brian.timko@tufts.edu

Authors

Corey P. Fucetola – Department of Biomedical Engineering, Tufts University, Medford, Massachusetts 02155, United States;  orcid.org/0000-0002-8657-8537

Justin T. Wang – Department of Biomedical Engineering, Tufts University, Medford, Massachusetts 02155, United States;  orcid.org/0000-0001-7969-2457

Olurotimi A. Bolonduro – Department of Biomedical Engineering, Tufts University, Medford, Massachusetts 02155, United States;  orcid.org/0000-0002-3210-0650

Complete contact information is available at:

<https://pubs.acs.org/10.1021/acsnano.3c11841>

Author Contributions

B.P.T. collected the data and directed the study. C.P.F., J.W., C.M.L., and B.P.T. analyzed the data and wrote the manuscript. C.P.F., J.W., O.A.B., and B.P.T. designed, built, and maintained CVD facilities. All authors have given approval to the final version of the manuscript.

Funding

B.P.T. acknowledges support from the NSF (CAREER Award 2239557), AHA (Transformational Project Award 23TPA1057212), and NIH/NIBIB (R21EB034527)

Notes

The authors declare no competing financial interest.

ACKNOWLEDGMENTS

We thank D. Bell and A. Auslender for assistance with microscopy and A. Wissner-Gross, W. Lu, and A. Greytak for helpful conversations. This work was performed in part at Harvard University and the Harvard University Center for Nanoscale Systems (CNS). CNS is a member of the National Nanotechnology Coordinated Infrastructure Network (NNCI), which is supported by the National Science Foundation under NSF award no. ECCS-2025158.

ABBREVIATIONS

CVD, Chemical Vapor Deposition; TEM, Transmission Electron Microscopy; FET, Field-effect Transistor

REFERENCES

- (1) Park, M. H.; Kim, M. G.; Joo, J.; Kim, K.; Kim, J.; Ahn, S.; Cui, Y.; Cho, J. Silicon nanotube battery anodes. *Nano Lett.* **2009**, *9* (11), 3844–3847.
- (2) Wu, H.; Chan, G.; Choi, J. W.; Ryu, I.; Yao, Y.; McDowell, M. T.; Lee, S. W.; Jackson, A.; Yang, Y.; Hu, L.; Cui, Y. Stable cycling of double-walled silicon nanotube battery anodes through solid-electrolyte interphase control. *Nat. Nanotechnol.* **2012**, *7* (5), 310–315.
- (3) Liu, H. T.; Haider, B.; Fried, H. R.; Ju, J.; Bolonduro, O.; Raghuram, V.; Timko, B. P. Nanobiotechnology: 1D nanomaterial building blocks for cellular interfaces and hybrid tissues. *Nano Res.* **2018**, *11* (10), 5372–5399.
- (4) Acaron Ledesma, H.; Li, X.; Carvalho-de-Souza, J. L.; Wei, W.; Bezanilla, F.; Tian, B. An atlas of nano-enabled neural interfaces. *Nat. Nanotechnol.* **2019**, *14* (7), 645–657.
- (5) Fang, J.; Xu, D.; Wang, H.; Wu, J.; Li, Y.; Yang, T.; Liu, C.; Hu, N. Scalable and Robust Hollow Nanopillar Electrode for Enhanced Intracellular Action Potential Recording. *Nano Lett.* **2023**, *23* (1), 243–251.
- (6) Lin, Z. C.; Xie, C.; Osakada, Y.; Cui, Y.; Cui, B. Iridium oxide nanotube electrodes for sensitive and prolonged intracellular measurement of action potentials. *Nat. Commun.* **2014**, *5*, 3206.
- (7) Zhang, A.; Lieber, C. M. Nano-Bioelectronics. *Chem. Rev.* **2016**, *116* (1), 215–257.
- (8) Wang, Y.; Zhao, Y.; Bollas, A.; Wang, Y.; Au, K. F. Nanopore sequencing technology, bioinformatics and applications. *Nat. Biotechnol.* **2021**, *39* (11), 1348–1365.
- (9) Peinetti, A. S.; Lake, R. J.; Cong, W.; Cooper, L.; Wu, Y.; Ma, Y.; Pawel, G. T.; Toimil-Molares, M. E.; Trautmann, C.; Rong, L.; et al. Direct detection of human adenovirus or SARS-CoV-2 with ability to inform infectivity using DNA aptamer-nanopore sensors. *Sci. Adv.* **2021**, *7* (39), eab2848.
- (10) Jiang, X. J.; Wang, L.; Liu, S. D.; Li, F.; Liu, J. Q. Bioinspired artificial nanochannels: construction and application. *Mater. Chem. Front.* **2021**, *5* (4), 1610–1631.
- (11) Martin, C. R. Nanomaterials - a Membrane-Based Synthetic Approach. *Science* **1994**, *266* (5193), 1961–1966.
- (12) Liu, Y. L.; Zhu, J.; Weng, G. J.; Li, J. J.; Zhao, J. W. Gold nanotubes: synthesis, properties and biomedical applications. *Mikrochim. Acta* **2020**, *187* (11), 612.
- (13) Lakshmi, B. B.; Patrissi, C. J.; Martin, C. R. Sol-gel template synthesis of semiconductor oxide micro- and nanostructures. *Chem. Mater.* **1997**, *9* (11), 2544–2550.
- (14) Hwang, J.; Min, B. D.; Lee, J. S.; Keem, K.; Cho, K.; Sung, M. Y.; Lee, M. S.; Kim, S. Al₂O₃ nanotubes fabricated by wet etching of ZnO/Al₂O₃ core/shell nanofibers. *Adv. Mater.* **2004**, *16* (5), 422.
- (15) Yada, M.; Mihara, M.; Mouri, S.; Kuroki, M.; Kijima, T. Rare earth (Er, Tm, Yb, Lu) oxide nanotubes templated by dodecylsulfate assemblies. *Adv. Mater.* **2002**, *14* (4), 309.
- (16) Zou, J. P.; Pu, L.; Bao, X. M.; Feng, D. Branchy alumina nanotubes. *Appl. Phys. Lett.* **2002**, *80* (6), 1079–1081.
- (17) Jeong, S. Y.; Kim, J. Y.; Yang, H. D.; Yoon, B. N.; Choi, S. H.; Kang, H. K.; Yang, C. W.; Lee, Y. H. Synthesis of silicon nanotubes on porous alumina using molecular beam epitaxy. *Adv. Mater.* **2003**, *15* (14), 1172.
- (18) Sha, J.; Niu, J. J.; Ma, X. Y.; Xu, J.; Zhang, X. B.; Yang, Q.; Yang, D. Silicon nanotubes. *Adv. Mater.* **2002**, *14* (17), 1219.
- (19) Hu, J. Q.; Bando, Y.; Liu, Z. W.; Zhan, J. H.; Golberg, D.; Sekiguchi, T. Synthesis of crystalline silicon tubular nanostructures with ZnS nanowires as removable templates. *Angew. Chem. Int. Ed.* **2004**, *43* (1), 63–66.
- (20) Pham-Huu, C.; Keller, N.; Ehret, G.; Ledoux, M. J. The first preparation of silicon carbide nanotubes by shape memory synthesis and their catalytic potential. *J. Catal.* **2001**, *200* (2), 400–410.
- (21) Hu, J. Q.; Bando, Y.; Golberg, D.; Liu, Q. L. Gallium nitride nanotubes by the conversion of gallium oxide nanotubes. *Angew. Chem. Int. Ed.* **2003**, *42* (30), 3493–3497.
- (22) Goldberger, J.; He, R.; Zhang, Y.; Lee, S.; Yan, H.; Choi, H. J.; Yang, P. Single-crystal gallium nitride nanotubes. *Nature* **2003**, *422* (6932), 599–602.
- (23) Mohan, P.; Motohisa, J.; Fukui, T. Realization of conductive InAs nanotubes based on lattice-mismatched InP/InAs core-shell nanowires. *Appl. Phys. Lett.* **2006**, *88* (1), No. 013110, DOI: [10.1063/1.2161576](https://doi.org/10.1063/1.2161576).
- (24) Bakkers, E. P. A. M.; Verheijen, M. A. Synthesis of InP nanotubes. *J. Am. Chem. Soc.* **2003**, *125* (12), 3440–3441.
- (25) Patolsky, F.; Zheng, G.; Lieber, C. M. Fabrication of silicon nanowire devices for ultrasensitive, label-free, real-time detection of biological and chemical species. *Nat. Protoc.* **2006**, *1* (4), 1711–1724.
- (26) Daiguji, H.; Yang, P. D.; Majumdar, A. Ion transport in nanofluidic channels. *Nano Lett.* **2004**, *4* (1), 137–142.

- (27) Karnik, R.; Fan, R.; Yue, M.; Li, D. Y.; Yang, P. D.; Majumdar, A. Electrostatic control of ions and molecules in nanofluidic transistors. *Nano Lett.* **2005**, *5* (5), 943–948.
- (28) Daiguji, H.; Oka, Y.; Shirono, K. Nanofluidic diode and bipolar transistor. *Nano Lett.* **2005**, *5* (11), 2274–2280.
- (29) Karnik, R.; Castelino, K.; Fan, R.; Yang, P.; Majumdar, A. Effects of biological reactions and modifications on conductance of nanofluidic channels. *Nano Lett.* **2005**, *5* (9), 1638–1642.
- (30) Gao, R. X.; Strehle, S.; Tian, B. Z.; Cohen-Karni, T.; Xie, P.; Duan, X. J.; Qing, Q.; Lieber, C. M. Outside Looking In: Nanotube Transistor Intracellular Sensors. *Nano Lett.* **2012**, *12* (6), 3329–3333.
- (31) Koch, M.; Evans, A.; Brunnenschweiler, A. Microfluidic Devices I: Flow Control. In *Microfluidic technology and applications*; Research Studies Press: Philadelphia, PA, 2000; pp 151–215.
- (32) Mitchell, D. T.; Lee, S. B.; Trofin, L.; Li, N. C.; Nevanen, T. K.; Söderlund, H.; Martin, C. R. Smart nanotubes for bioseparations and biocatalysis. *J. Am. Chem. Soc.* **2002**, *124* (40), 11864–11865.
- (33) Lu, W.; Xiang, J.; Timko, B. P.; Wu, Y.; Lieber, C. M. One-dimensional hole gas in germanium/silicon nanowire heterostructures. *P Natl. Acad. Sci. USA* **2005**, *102* (29), 10046–10051.
- (34) Wang, R.; Deacon, R. S.; Sun, J.; Yao, J.; Lieber, C. M.; Ishibashi, K. Gate Tunable Hole Charge Qubit Formed in a Ge/Si Nanowire Double Quantum Dot Coupled to Microwave Photons. *Nano Lett.* **2019**, *19* (2), 1052–1060.
- (35) Primak, W.; Kampwirth, R.; Dayal, Y. Peroxide Etching of Germanium. *J. Electrochem. Soc.* **1967**, *114* (1), 88.
- (36) Wu, Y.; Cui, Y.; Huynh, L.; Barrelet, C. J.; Bell, D. C.; Lieber, C. M. Controlled growth and structures of molecular-scale silicon nanowires. *Nano Lett.* **2004**, *4* (3), 433–436.
- (37) Shur, M. Basic Semiconductor Physics. *Physics of semiconductor devices*; Prentice Hall: Upper Saddle River, NJ, 1990; pp 10–25.
- (38) Cui, Y.; Duan, X. F.; Hu, J. T.; Lieber, C. M. Doping and electrical transport in silicon nanowires. *J. Phys. Chem. B* **2000**, *104* (22), 5213–5216.
- (39) Cui, Y.; Zhong, Z. H.; Wang, D. L.; Wang, W. U.; Lieber, C. M. High performance silicon nanowire field effect transistors. *Nano Lett.* **2003**, *3* (2), 149–152.
- (40) Pierson, H. O. Fundamentals of Chemical Vapor Deposition. In *Handbook of chemical vapor deposition: principles, technology, and applications*; Noyes Publications: Westwood, NJ, 1999; pp 26–35.
- (41) Nakane, J. J.; Akeson, M.; Marziani, A. Nanopore sensors for nucleic acid analysis. *J. Phys.-Condens Mat.* **2003**, *15* (32), R1365–R1393.
- (42) Bush, S. N.; Volta, T. T.; Martin, C. R. Chemical Sensing and Chemoresponsive Pumping with Conical-Pore Polymeric Membranes. *Nanomaterials (Basel)* **2020**, *10* (3), 571.
- (43) Ojovan, S. M.; Rabieh, N.; Shmoel, N.; Erez, H.; Maydan, E.; Cohen, A.; Spira, M. E. A feasibility study of multi-site,intracellular recordings from mammalian neurons by extracellular gold mushroom-shaped microelectrodes. *Sci. Rep.* **2015**, *5*, 14100.
- (44) Bocquet, L. Nanofluidics coming of age. *Nat. Mater.* **2020**, *19* (3), 254–256.
- (45) Wang, D.; Qian, F.; Yang, C.; Zhong, Z. H.; Lieber, C. M. Rational growth of branched and hyperbranched nanowire structures. *Nano Lett.* **2004**, *4* (5), 871–874.
- (46) Dick, K. A.; Deppert, K.; Larsson, M. W.; Mårtensson, T.; Seifert, W.; Wallenberg, L. R.; Samuelson, L. Synthesis of branched ‘nanotrees’ by controlled seeding of multiple branching events. *Nat. Mater.* **2004**, *3* (6), 380–384.
- (47) Ge, S. P.; Jiang, K. L.; Lu, X. X.; Chen, Y. F.; Wang, R. M.; Fan, S. S. Orientation-controlled growth of single-crystal silicon-nanowire arrays. *Adv. Mater.* **2005**, *17* (1), 56.
- (48) Tian, B.; Cohen-Karni, T.; Qing, Q.; Duan, X.; Xie, P.; Lieber, C. M. Three-dimensional, flexible nanoscale field-effect transistors as localized bioprobes. *Science* **2010**, *329* (5993), 830–834.
- (49) Zimmerman, J. F.; Parameswaran, R.; Murray, G.; Wang, Y.; Burke, M.; Tian, B. Cellular uptake and dynamics of unlabeled freestanding silicon nanowires. *Sci. Adv.* **2016**, *2* (12), e1601039.
- (50) Lee, J. H.; Zhang, A.; You, S. S.; Lieber, C. M. Spontaneous Internalization of Cell Penetrating Peptide-Modified Nanowires into Primary Neurons. *Nano Lett.* **2016**, *16* (2), 1509–1513.
- (51) Parameswaran, R.; Koehler, K.; Rotenberg, M. Y.; Burke, M. J.; Kim, J.; Jeong, K. Y.; Hissa, B.; Paul, M. D.; Moreno, K.; Sarma, N.; et al. Optical stimulation of cardiac cells with a polymer-supported silicon nanowire matrix. *Proc. Natl. Acad. Sci. U. S. A.* **2019**, *116* (2), 413–421.
- (52) Yu, G. H.; Lieber, C. M. Assembly and integration of semiconductor nanowires for functional nanosystems. *Pure Appl. Chem.* **2010**, *82* (12), 2295–2314.
- (53) Zhao, Y.; Yao, J.; Xu, L.; Mankin, M. N.; Zhu, Y.; Wu, H.; Mai, L.; Zhang, Q.; Lieber, C. M. Shape-Controlled Deterministic Assembly of Nanowires. *Nano Lett.* **2016**, *16* (4), 2644–2650.
- (54) Li, M.; Bhiladvala, R. B.; Morrow, T. J.; Sioss, J. A.; Lew, K. K.; Redwing, J. M.; Keating, C. D.; Mayer, T. S. Bottom-up assembly of large-area nanowire resonator arrays. *Nat. Nanotechnol.* **2008**, *3* (2), 88–92.
- (55) Yao, J.; Yan, H.; Lieber, C. M. A nanoscale combing technique for the large-scale assembly of highly aligned nanowires. *Nat. Nanotechnol.* **2013**, *8* (5), 329–335.
- (56) Gao, H.; Yin, B.; Wu, S.; Liu, X.; Fu, T.; Zhang, C.; Lin, J.; Yao, J. Deterministic Assembly of Three-Dimensional Suspended Nanowire Structures. *Nano Lett.* **2019**, *19* (8), 5647–5652.
- (57) Yao, J.; Yan, H.; Das, S.; Klemic, J. F.; Ellenbogen, J. C.; Lieber, C. M. Nanowire nanocomputer as a finite-state machine. *P Natl. Acad. Sci. USA* **2014**, *111* (7), 2431–2435.
- (58) Dey, S.; Fan, C. H.; Gothelf, K. V.; Li, J.; Lin, C. X.; Liu, L. F.; Liu, N.; Nijenhuis, M. A. D.; Saccà, B.; Simmel, F. C.; et al. DNA origami. *Nat. Rev. Methods Primers* **2021**, *1* (1), DOI: 10.1038/s43586-020-00009-8.
- (59) Ke, Y.; Ong, L. L.; Shih, W. M.; Yin, P. Three-dimensional structures self-assembled from DNA bricks. *Science* **2012**, *338* (6111), 1177–1183.
- (60) Sun, W.; Shen, J.; Zhao, Z.; Arellano, N.; Rettner, C.; Tang, J. S.; Cao, T. Y.; Zhou, Z. Y.; Ta, T.; Streit, J. K.; et al. Precise pitch-scaling of carbon nanotube arrays within three-dimensional DNA nanotrenches. *Science* **2020**, *368* (6493), 874.
- (61) Tian, B.; Kempa, T. J.; Lieber, C. M. Single nanowire photovoltaics. *Chem. Soc. Rev.* **2009**, *38* (1), 16–24.
- (62) Zhou, W.; Dai, X.; Fu, T. M.; Xie, C.; Liu, J.; Lieber, C. M. Long term stability of nanowire nanoelectronics in physiological environments. *Nano Lett.* **2014**, *14* (3), 1614–1619.
- (63) Yang, X.; Forro, C.; Li, T. L.; Miura, Y.; Zaluska, T. J.; Tsai, C. T.; Kanton, S.; McQueen, J. P.; Chen, X.; Mollo, V.; et al. Kirigami electronics for long-term electrophysiological recording of human neural organoids and assembloids. *bioRxiv* (neuroscience). DOI: 10.1101/2023.09.22.559050 (accessed 2023-12-26).
- (64) Kalmykov, A.; Huang, C.; Bliley, J.; Shiawski, D.; Tashman, J.; Abdullah, A.; Rastogi, S. K.; Shukla, S.; Mataev, E.; Feinberg, A. W.; et al. Organ-on-a-chip: Three-dimensional self-rolled biosensor array for electrical interrogations of human electrogenic spheroids. *Sci. Adv.* **2019**, *5* (8), eaax0729.
- (65) Song, E. M.; Li, J. H.; Won, S. M.; Bai, W. B.; Rogers, J. A. Materials for flexible bioelectronic systems as chronic neural interfaces. *Nat. Mater.* **2020**, *19* (6), 590–603.
- (66) Zhang, A.; Mandeville, E. T.; Xu, L.; Stary, C. M.; Lo, E. H.; Lieber, C. M. Ultraflexible endovascular probes for brain recording through micrometer-scale vasculature. *Science* **2023**, *381* (6655), 306–312.
- (67) Timko, B. P. Neural implants without brain surgery. *Science* **2023**, *381* (6655), 268–269.
- (68) Cui, Y.; Lauhon, L. J.; Gudiksen, M. S.; Wang, J. F.; Lieber, C. M. Diameter-controlled synthesis of single-crystal silicon nanowires. *Appl. Phys. Lett.* **2001**, *78* (15), 2214–2216.
- (69) Gudiksen, M. S.; Lauhon, L. J.; Wang, J.; Smith, D. C.; Lieber, C. M. Growth of nanowire superlattice structures for nanoscale photonics and electronics. *Nature* **2002**, *415* (6872), 617–620.

- (70) Cui, Y.; Lieber, C. M. Functional nanoscale electronic devices assembled using silicon nanowire building blocks. *Science* **2001**, *291* (5505), 851–853.
- (71) Lu, W.; Xiang, J.; Timko, B. P.; Wu, Y.; Lieber, C. M. One-dimensional hole gas in germanium/silicon nanowire heterostructures. *Proc. Natl. Acad. Sci. U. S. A.* **2005**, *102* (29), 10046–10051.
- (72) Martel, R.; Schmidt, T.; Shea, H. R.; Hertel, T.; Avouris, P. Single- and multi-wall carbon nanotube field-effect transistors. *Appl. Phys. Lett.* **1998**, *73* (17), 2447–2449.



CAS BIOFINDER DISCOVERY PLATFORM™

BRIDGE BIOLOGY AND CHEMISTRY FOR FASTER ANSWERS

Analyze target relationships,
compound effects, and disease
pathways

Explore the platform

